

# Tunneling-induced restoration of classical degeneracy in quantum kagome ice

Kai-Hsin Wu,<sup>1</sup> Yi-Ping Huang,<sup>2</sup> and Ying-Jer Kao<sup>1,3,\*</sup>

<sup>1</sup>*Department of Physics and Center for Theoretical Physics, National Taiwan University, Taipei 10607, Taiwan*

<sup>2</sup>*Max Planck Institute for the Physics of Complex Systems, D-01187 Dresden, Germany*

<sup>3</sup>*National Center for Theoretical Sciences, National Tsing Hua University, Hsin-Chu 30013, Taiwan*  
(Dated: December 14, 2024)

Quantum effect is expected to dictate the behaviour of physical systems at low temperature. For quantum magnets with geometrical frustration, quantum fluctuation lifts the macroscopic classical degeneracy, and exotic quantum states emerge. However, how different types of quantum processes entangle wave functions in a constrained Hilbert space is not well understood. Here, we study the topological entanglement entropy (TEE) and the thermal entropy of a quantum ice model on a geometrically frustrated kagome lattice. We find that the system does not show a  $Z_2$  topological order down to extremely low temperatures, yet continues to behave like a classical kagome ice with finite residual entropy. Our theoretical analysis indicates that an intricate competition of off-diagonal and diagonal quantum tunneling processes leading to a suppression of the quantum energy scale. This new paradigm suggests quantum spin ice materials can be engineered to study the novel quantum-classical transition.

In systems with macroscopic ground state degeneracy, quantum correlation introduces non-trivial constraints on the Hilbert space, leading to the emergence of highly entangled quantum states of matter. The scenario is the gist in the studies of quantum Hall effect [1], flat band physics [2–4] and quantum spin liquids [5–11]. Among them, quantum magnets with geometrical frustration have become a fruitful playground to search for exotic quantum phases. In particular, spin ice systems on the corner-sharing tetrahedron lattices have attracted enormous attention due to their relevance to rare-earth pyrochlore materials [8, 10–12] and the possibility to explore exotic quantum states of matter with anisotropic quantum exchange [13–21].

Strong spin-orbit couplings in these materials lead to relatively unexplored anisotropic quantum effects. Dominant ferromagnetic Ising coupling in spin ice materials aligns spins along the local  $\langle 111 \rangle$  directions on the tetrahedron and becomes geometrically frustrated at low temperatures. The macroscopically degenerate ground states obey the so-called “ice rules”, with two spins pointing in and two spins pointing out of the centre of each tetrahedron. By introducing different quantum tunneling processes, spin ice systems could be

driven into various exotic quantum phases [13–16, 21].

In addition to the intriguing physics in three dimensions, these pyrochlore spin ice materials also serve as a playground for studying quantum ice physics on a kagome lattice. The pyrochlore lattice can be visualized as alternating layers of triangular and kagome lattice stacking along the  $[111]$  direction (Fig. 1a). When an external field along this axis pins the spins on the triangular layer, effectively the system becomes decoupled layers of two-dimensional (2D) kagome lattices, provided the field is not too strong. This dimensional reduction partially reduces the degeneracy and the ice rule is modified to the kagome ice rule with two spins pointing into each triangle, and one out (2-up-1-down in terms of the pseudo-spin), or vice versa, as shown in Fig. 1b.

Recently, numerical simulation on the kagome lattice focusing on the pair-flipping process finds a gapped disordered quantum state, dubbed as quantum kagome ice (QKI), which is argued to be an exotic  $Z_2$  QSL [22]; however, direct evidence characterising the non-trivial entanglement pattern in the ground state, such as the TEE, has not been analysed. Furthermore, how these pair-flipping processes should manifest the anisotropic nature within the ice manifold is not fully explored. Using large-scale quantum Monte Carlo (QMC) simulations and degenerate perturbation theory (DPT), we show that the QKI state does not show a  $Z_2$  topological order, but continues to behave like a classical kagome ice (CKI) due to the competition among different quantum tunneling processes. These results suggest that by tuning the weight of different quantum processes, spin ice pyrochlore materials subject to an external field can be used to study novel quantum-classical transitions [23].

## I. RESULTS

**Quantum kagome ice model with pair-flipping interaction**— On a kagome lattice, the nearest-neighbour, symmetry-allowed exchange interactions for the ground state doublets can be modeled with an effective pseudo-spin-1/2 XYZh model [22],

$$H_{\text{XYZh}} = \sum_{\langle \mathbf{r}, \mathbf{r}' \rangle} J_z S_{\mathbf{r}}^z S_{\mathbf{r}'}^z - h \sum_{\mathbf{r}} S_{\mathbf{r}}^z - \sum_{\langle \mathbf{r}, \mathbf{r}' \rangle} \frac{J_{\pm}}{2} (S_{\mathbf{r}}^+ S_{\mathbf{r}'}^- + S_{\mathbf{r}}^- S_{\mathbf{r}'}^+) + \frac{J_{\pm\pm}}{2} (S_{\mathbf{r}}^+ S_{\mathbf{r}'}^+ + S_{\mathbf{r}}^- S_{\mathbf{r}'}^-) \quad (1)$$

\* yjkao@phys.ntu.edu.tw

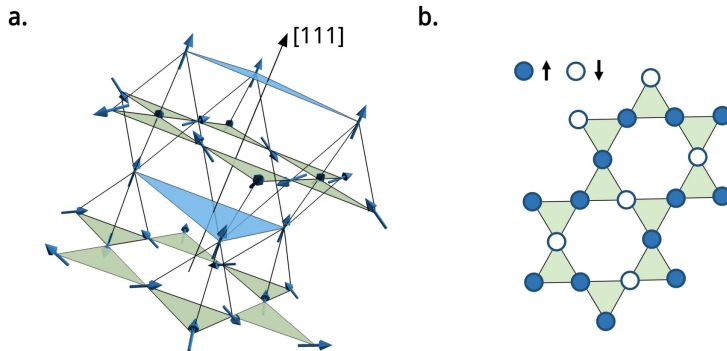


FIG. 1: **Geometry of pyrochlore lattice and the kagome layer.** **a.** A pyrochlore spin ice consists of corner sharing tetrahedra of spins pointing into or out of each tetrahedron. The ferromagnetic coupling between nearest-neighbour spins leads to geometrical frustration, where spins on each tetrahedron follow a '2-in-2-out' ice rule. Pinning the spin on the triangular layers by applying a strong enough field along the [111] direction reduces the pyrochlore lattice to decoupled kagome layers (green layers). **b.** Kagome lattice can be viewed as corner-sharing triangles, or equivalently, corner-sharing hexagons. In a field, pseudo-spins on each triangle satisfies the kagome ice rule with '2-up-1-down' or '2-down-1-up' depending on the sign of the field ( $h > 0$  here).

where  $J_z > 0$ ,  $\mathbf{r}$  labels kagome lattice sites, and  $\langle \mathbf{r}, \mathbf{r}' \rangle$  denotes the nearest-neighbour pairs. The first two terms correspond to the CKI model in a field, the third term corresponds to the quantum exchange and the last term is the pair-flipping interaction. In the following, we set  $J_z = 1$  unless explicitly stated otherwise.

For  $J_{\pm\pm} = 0$  and  $J_{\pm} > 0$ , this model is equivalent to the XXZ model. Previous studies show the ground state is a valence-bond solid (VBS) phase with a three-fold degeneracy [24, 25]. With  $J_{\pm} = 0$  and  $J_{\pm\pm} < 0$ , recently the model is proposed to harbour a  $Z_2$  QSL both numerically [22] and theoretically [26]. Note that the parameter space of  $J_{\pm\pm} > 0$  and  $J_{\pm\pm} < 0$  are physically equivalent, connected via a unitary transformation  $S^+ \rightarrow iS^+$ . Without loss of generality, we will analyse model (1) with  $J_{\pm\pm} < 0$ .

**Topological entanglement entropy**— For a quantum system with short-range interaction, the Renyi entanglement entropies between subregions  $A$  and  $B$  obeys the so-called *area law*,

$$S_n(A) = \kappa l - \alpha \gamma + O(L^{-1}), \quad (2)$$

where  $\kappa$  is a non-universal constant and  $l$  is the boundary length of the subregion.  $\gamma$  is the TEE and  $\alpha$  is related to the number of (disconnected) boundaries. As a universal constant, the TEE plays the role of "order parameter" for detecting the hidden topological order in the system [27, 28]. The value of the TEE is related to the quantum dimension  $\mathcal{D}$  with  $\gamma = \ln \mathcal{D}$  that characterises the quasi-particle fractionalization of the topological order [27]. For a system with a  $Z_2$  topological order, the quantum dimension  $\mathcal{D} = 2$ , and we expect  $\gamma = \ln 2$  [29, 30].

We measure the quantum entanglement using the second Renyi entropy [31, 32],

$$S_2(A) = -\ln \text{Tr}(\rho_A^2), \quad (3)$$

where  $\rho_A$  is the reduced density matrix of subregion  $A$ . Using the replica trick [31], we measure  $S_2$  with four different subregions (Fig. 2a) that are strategically designed to eliminate the area terms [28], and

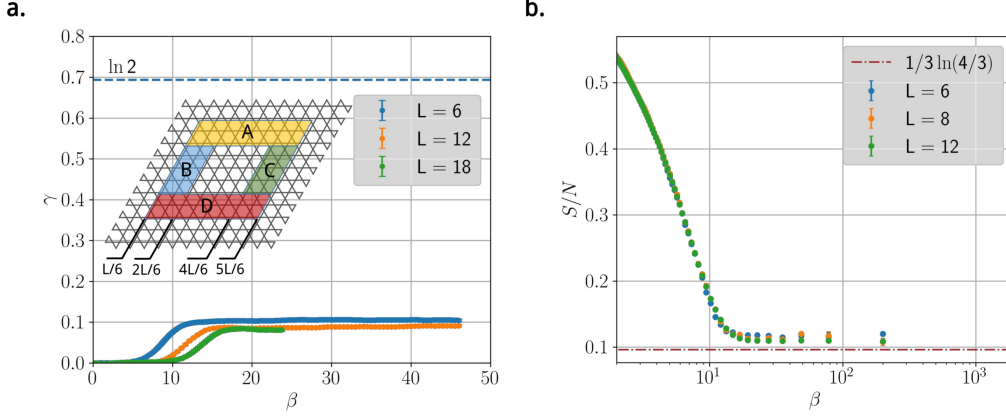
$$2\gamma = -S_2(R_1) - S_2(R_2) + S_2(R_3) + S_2(R_4). \quad (4)$$

Fig. 2a shows TEE as a function of the inverse temperature  $\beta = 1/T$  with parameters in the QKI regime ( $J_{\pm\pm} = -0.49$ ,  $J_{\pm} = 0$ , and  $h = 0.833$ ). We find  $\gamma$  is far below the expected  $\ln 2$  value even at temperature as low as  $T \approx 1/48$  ( $\beta = 48$ ), indicating the system does not have a  $Z_2$  topological order. The small finite  $\gamma$  at low temperature is due to sub-leading corrections that cannot be cancelled. This result suggests two possibilities: either the QKI state is a short-range entangled symmetry protected topological order or the quantum fluctuations couple different kagome ice states in such a manner that the system behaves classically. We clarify this issue through the study of thermal entropy at low temperature.

**Thermal entropy**— The ground states of the XYZh model (1) in the classical limit satisfy the 2-up-1-down kagome ice rule and are extensively degenerate, leading to a residual entropy per spin  $S/N = 1/3 \ln(4/3)$  [33].

In order to directly measure the thermal entropy in our QMC simulations, we employ the Wang-Landau method [34]. We observe at extremely low temperature  $T = 1/200$  ( $\beta = 200$ ), the thermal entropy remains finite and the value corresponds to the residual entropy per spin of a CKI. This classical behaviour in the quantum region is counter-intuitive. The system neither enters an ordered phase through the quantum order-by-disorder scheme [35–37] nor becomes a highly entangled disordered quantum state. To solve this puzzle, we analyse possible quantum processes out of the CKI manifold using DPT [38, 39].

**Degenerate Perturbation Theory**— Starting from the classical model, we treat all the quantum fluctuations as per-



**FIG. 2: Topological entanglement entropy and thermal entropy.** **a.** Topological entanglement entropy (TEE) as a function of the inverse temperature  $\beta = 1/T$  with parameters in the QKI phase ( $J_{\pm\pm} = -0.49$ ,  $J_{\pm} = 0$ , and  $h = 0.833$ ). The system size is  $N=3 \times L \times L$ .  $\gamma$  converges to a value far smaller than  $\ln 2$  (blue horizontal line), indicating the system does not show a  $Z_2$  topological order. Four regions in Eq. (4) are defined as  $R_1 \equiv A \cup B \cup D$ ,  $R_2 \equiv A \cup C \cup D$ ,  $R_3 \equiv A \cup B \cup C \cup D$  and  $R_4 \equiv A \cup D$ . **b.** Thermal entropy per spin  $S/N$  as a function of  $\beta$  in the QKI phase ( $J_{\pm\pm} = -0.45$ ,  $J_{\pm} = 0$ ,  $h = 1$ ). The low temperature plateau is consistent with the residual entropy per spin of a CKI (brown horizontal dot-dashed line).

turbations. It is useful in the following analysis to view the kagome lattice as corner-sharing hexagons; thus, all the non-trivial perturbation processes are within a single star of David (Fig. 3a). The presence of the field splits the degeneracy of the kagome ice rule on each triangle, and the 2-up-1-down configurations are favoured. Spin configuration on each star is therefore uniquely determined by the hexagon configuration (Fig. 3b) that determines the process in the perturbation theory.

First, we consider the case  $J_{\pm\pm} \neq 0$  and  $J_{\pm} = 0$  where the proposed QKI is realised. The leading non-trivial processes appear at the sixth-order of perturbation, and an effective Hamiltonian  $\hat{P}_6$  can be written as,

$$\begin{aligned} \hat{P}_6 &= H_d + K_{pp} \sum_{\forall \square n=3} H_{\square, n=3}, & (5) \\ H_d &= D_4 \sum_{\forall \square n=4} H_{\square, n=4} \\ &+ D_5 \sum_{\forall \square n=5} H_{\square, n=5} \\ &+ D_6 \sum_{\forall \square n=6} H_{\square, n=6}. & (6) \end{aligned}$$

$H_{\square, n=3}$  acts on an  $n=3$  hexagon to generate an effective ring-exchange process, as shown in Fig. 3c, which brings one CKI configuration to a different one. In addition to the ring-exchange term, various non-trivial diagonal terms  $H_d$  appear at the same order of perturbation acting on hexagons  $n \geq 4$  (Fig. 3d). The coefficients of these processes can be directly computed in DPT (See Appendix for details). In the case of  $h = J_z$ , we have  $K_{pp} = -\frac{58}{81}\Gamma$ ,  $D_4 = -\frac{1}{36}\Gamma$ ,  $D_5 = -\frac{289}{5292}\Gamma$ ,  $D_6 = -\frac{2}{49}\Gamma$ , where  $\Gamma = J_{\pm\pm}^6/J_z^5$ .

Consider the other limiting case where  $J_{\pm} \neq 0$  and  $J_{\pm\pm} = 0$ . The lowest non-trivial process occurs at the third order of

perturbation, with an effective Hamiltonian,

$$\hat{P}_3 = K_{np} \sum_{\forall \square n=3} H_{\square, n=3} + c, \quad (7)$$

where  $K_{np} = -12J_{\pm}^3/J_z^2$ . All diagonal processes at this level contribute to an overall constant energy shift  $c$  which is irrelevant. The ring-exchange term  $H_{\square, n=3}$  drives the system into a VBS ground state.

Figure 4a shows a schematic picture to illustrate the effects coming from the diagonal and off-diagonal quantum tunneling processes. For a QKI ( $J_{\pm\pm} \neq 0$  and  $J_{\pm} = 0$ ), the introduction of the off-diagonal ring-exchange  $H_{\square, n=3}$  selects the three-fold degenerate VBS state out of the degenerate classical ice manifold, leaving all other states at higher energies. Adding the diagonal terms, reconfiguration of the energy levels occurs. These terms tend to maximise the overall fraction of  $n=4, 5, 6$  hexagons while minimising the fraction of  $n=3$  hexagons. The competition between diagonal and off-diagonal processes reorganises the states into quasi-degenerate levels and the classical degeneracy is restored. On the other hand, for the case  $J_{\pm} \neq 0$  and  $J_{\pm\pm} = 0$ , the process terminates at the ring-exchange level, and the VBS ground state is selected.

We further demonstrate this mechanism by measuring  $P_n$ , the fraction of hexagons with  $n$  up spins using QMC (Fig. 4b). For the VBS parameters, the weight of  $n=3$  hexagons  $P_3$  dramatically increases at low temperature, accompanied by the decrease of  $P_4$ . On the other hand, for the QKI state, the fractions for each type of hexagons remain unchanged, suggesting the system remains within the CKI state down to temperature much lower than the perturbative energy scale. Although DPT is expected to work only in the small  $J_{\pm\pm}/J_z$  limit, this indicates the competition between these quantum tunneling processes is indeed nonperturbative.

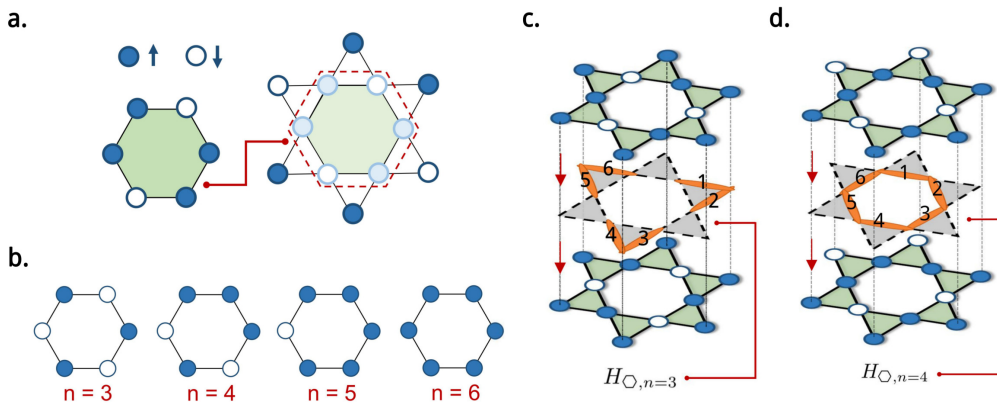


FIG. 3: **Hexagon units and quantum tunneling processes.** **(a)** In a field, spins on each triangle follow the 2-up-1-down rule. When the spin configuration on the hexagon is determined, the configuration of the remaining spins within the star of David is uniquely defined. **(b)** Four allowed hexagon configurations in a field, classified according to the number of up-spins  $n$ . **(c)** Example of the off-diagonal tunneling term  $H_{O,n=3}$  formed by six nearest-neighbour  $S^{\pm}S^{\pm}$  operators on the orange bonds that couples two different  $n = 3$  CKI states. **(d)** Example of the diagonal tunneling term  $H_{O,n=4}$  that couples the same  $n = 4$  CKI states.

With this physical picture in mind, we expect by tuning  $K_{pp}$  in the effective Hamiltonian (6), the VBS phase should emerge with large enough  $K_{pp}$ . This can be realized in the original XYZh model by including both nonzero  $J_{\pm}$  and  $J_{\pm\pm}$  terms. Since the VBS state breaks the translational symmetry, the structure factor should show peaks at ordering vector  $\mathbf{Q} = \langle \frac{2\pi}{3}, 0 \rangle$  and symmetry related momenta [24]. Figure 5 shows structure factors (see Supplemental Information for definition) for different parameters and the phase diagram in terms of  $h$ ,  $J_{\pm}$  and  $J_{\pm\pm}$ . With a small  $J_{\pm}$  term, the VBS phase becomes the ground state, as indicated by the peaks at the corner of the first Brillouin zone.

**Conclusions** Although the XYZh model on a kagome lattice has been proposed to be a new playground to search for 2D  $Z_2$  QSL, our results show that the QKI does not show a  $Z_2$  topological order at low temperature, and the system remains classical. The suppression of the quantum energy scale due to the competition between the off-diagonal ring-exchange and diagonal processes indicates that a much lower temperature than  $T = 1/200$  has to be reached before entering the true quantum regime. Even if the true quantum ground state is a  $Z_2$  QSL with an extremely small gap, it will be very hard to be realized experimentally or confirmed numerically since it is extremely fragile. Our results also indicate that the interpretation of recent experiments on  $\text{Nd}_2\text{Zr}_2\text{O}_7$  in a [111] field [40] as a *dynamical quantum kagome ice*, where the crystal field ground state are dipolar-octupolar Kramers doublets described by the pseudo-spin-1/2 XYZh model, should be taken with caution. On the other hand, although the true ground state remains unknown, it would be interesting to study the effects of tilting the field away from the [111] axis as this can provide an easy method to tune the ratio of the quantum processes. We finish by pointing out the non-trivial diagonal terms we found through DPT also exist on the pyrochlore lattice since the CKI states are a subset of the ice

manifold. Further systemic studies are necessary to see if the phenomena discussed in this paper can be extended to three dimensional cases [41, 42].

## II. METHODS

We implement the stochastic series expansion (SSE) [43, 44] in the  $S^z$  basis with a triangular plaquette break-up of the XYZh Hamiltonian. The directed loop equations are solved using numerical linear solver to minimize the bounce probability. The Renyi entanglement entropy is measured by implementing the replica trick [31]. In our simulations, we follow the scheme proposed in Ref. [45] to measure the second Renyi entanglement entropy  $S_2$  with four subregions independently. The simulation runs on average  $10^8 \sim 10^9$  Monte Carlo steps (MCS) for each subregion. The topological entanglement entropy  $\gamma$  is calculated by combining  $S_2$  of the four subregions with the standard bootstrap resampling procedure. The thermal entropy is measured with  $10^8$  MCS using SSE with the Wang-Landau algorithm [34] for a long operator string with a fixed length. The data presented in this paper requires the computation resources approximately about 330 CPU core-years on two different heterogeneous high-performance computers (HPCs) with 2.50GHz Intel Xeon or equivalent CPUs at the National Center for High-performance Computing.

## III. ACKNOWLEDGMENTS

This work was supported by the Ministry of Science and Technology (MOST) of Taiwan under Grants No. 105-2112-M-002-023-MY3, and 104-2112-M-002-022-MY3. We are grateful to the National Center for High-performance Com-

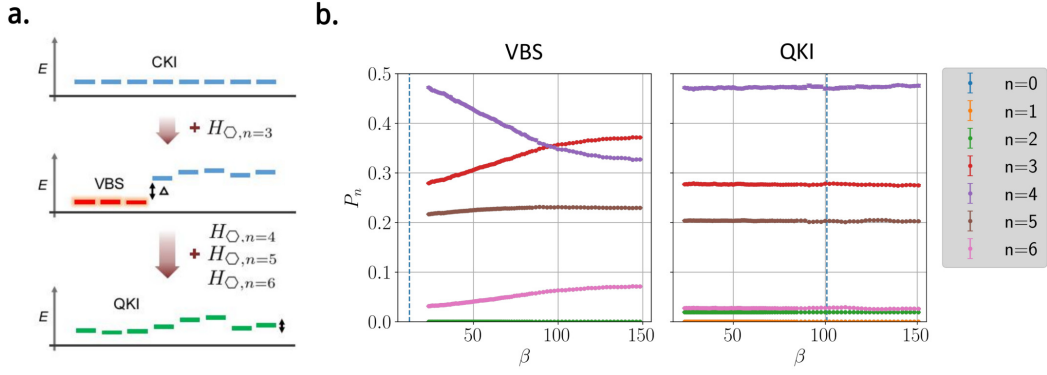


FIG. 4: **Effects of quantum tunneling processes.** **a.** The schematic picture of the energy level reorganisation due to the sixth-order perturbation (6). Starting from the degenerate classical ice manifold, we first introduce the ring-exchange term  $H_{\square, n=3}$ . This will select the three-fold degenerate VBS states with an energy gap  $\Delta$ . Further adding the diagonal terms  $H_{\square, n=4,5,6}$ , the energy levels are reorganised to become quasi-degenerate with a suppressed energy gap. **b.** QMC results of the hexagon fraction  $P_n$  vs  $\beta$  in the VBS regime with  $J_{\pm} = 0.19$  and  $J_{\pm\pm} = 0$  (left panel); and in the QKI regime  $J_{\pm\pm} = -0.49$  and  $J_{\pm} = 0$  (right panel). The vertical dashed line indicates the perturbative energy scale estimated by the leading ring-exchange contribution.

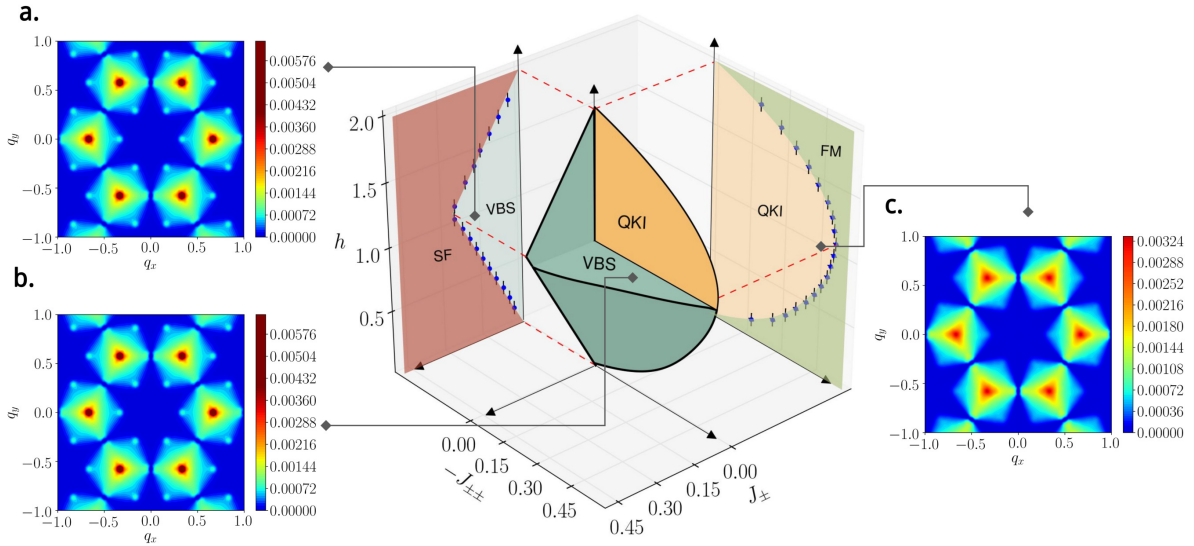


FIG. 5: **The phase diagram and structure factors** The schematic phase diagram shows possible phases of the XYZh model (1). The phase boundaries are guides to the eye. Projections to the  $J_{\pm} = 0$  and  $J_{\pm\pm} = 0$  planes are shown with the simulation data. Structure factors for three cases with **a.**  $J_{\pm\pm} = 0$ ,  $J_{\pm} = 0.19$  and  $h = 1.0$ , **b.**  $J_{\pm\pm} = -0.25$ ,  $J_{\pm} = 0.1219$ ,  $h = 1.0$ , and **c.**  $J_{\pm\pm} = -0.45$ ,  $J_{\pm} = 0$  and  $h = 1.0$ . In cases **a** and **b**, peaks are observed at  $\mathbf{Q} = \langle \frac{2\pi}{3}, 0 \rangle$  and symmetry related momenta, indicating the emergence of the VBS order; while in the QKI phase (case **c**), no peak is observed. The momentum vectors  $q_x$  and  $q_y$  are in unit of  $2\pi$ . The ferromagnetic peaks have been removed for clarity.

puting for computer time and facilities. Y.J.K. thanks Juan Carrasquilla, Mike Hermele and Zi-Yang Meng for useful discussions.

#### IV. AUTHOR CONTRIBUTIONS

K.H.W. and Y.J.K. conceived the numerical strategy. K.H.W. designed and programmed the algorithms, ran the simulation, and analysed the data. Y.P.H. and K.H.W. performed the degenerate perturbation theory analysis of the XYZh model. All three authors contributed to the writing of the manuscript and the interpretation of the results.

## V. ADDITIONAL INFORMATION

Correspondence and requests for materials should be addressed to Y.J.K.

## VI. COMPETING INTERESTS

The authors declare no competing financial interests.

- 
- [1] Richard E. Prange and Steven M. Girvin, *The Quantum Hall effect*, 2nd ed. (Springer-Verlag, New York, 1990.).
- [2] Evelyn Tang, Jia-Wei Mei, and Xiao-Gang Wen, “High-temperature fractional quantum hall states,” *Phys. Rev. Lett.* **106**, 236802 (2011).
- [3] Titus Neupert, Luiz Santos, Claudio Chamon, and Christopher Mudry, “Fractional quantum hall states at zero magnetic field,” *Phys. Rev. Lett.* **106**, 236804 (2011).
- [4] Kai Sun, Zhengcheng Gu, Hosho Katsura, and S. Das Sarma, “Nearly flatbands with nontrivial topology,” *Phys. Rev. Lett.* **106**, 236803 (2011).
- [5] P. W. Anderson, “Resonating valence bonds: A new kind of insulator?” *Mat. Res. Bull.* **8**, 153 (1973).
- [6] P. W. Anderson, “The resonating valence bond state in  $\text{La}_2\text{CuO}_4$  and superconductivity,” *Science* **235**, 1196 (1987).
- [7] R. Moessner and S. L. Sondhi, “Resonating valence bond phase in the triangular lattice quantum dimer model,” *Phys. Rev. Lett.* **86**, 1881–1884 (2001).
- [8] Michel JP Gingras and Paul A McClarty, “Quantum spin ice: a search for gapless quantum spin liquids in pyrochlore magnets,” *Reports on Progress in Physics* **77**, 056501 (2014).
- [9] Yi Zhou, Kazushi Kanoda, and Tai-Kai Ng, “Quantum spin liquid states,” *Rev. Mod. Phys.* **89**, 025003 (2017).
- [10] Lucile Savary and Leon Balents, “Quantum spin liquids: a review,” *Reports on Progress in Physics* **80**, 016502 (2016).
- [11] Johannes Knolle and Roderich Moessner, “A field guide to spin liquids,” (2018), arXiv:1804.02037 [cond-mat].
- [12] Jason S. Gardner, Michel J. P. Gingras, and John E. Greedan, “Magnetic pyrochlore oxides,” *Rev. Mod. Phys.* **82**, 53–107 (2010).
- [13] Michael Hermele, Matthew P. A. Fisher, and Leon Balents, “Pyrochlore photons: The  $U(1)$  spin liquid in a  $S = \frac{1}{2}$  three-dimensional frustrated magnet,” *Phys. Rev. B* **69**, 064404 (2004).
- [14] Lucile Savary and Leon Balents, “Coulombic quantum liquids in spin-1/2 pyrochlores,” *Phys. Rev. Lett.* **108**, 037202 (2012).
- [15] SungBin Lee, Shigeki Onoda, and Leon Balents, “Generic quantum spin ice,” *Phys. Rev. B* **86**, 104412 (2012).
- [16] Nic Shannon, Olga Sikora, Frank Pollmann, Karlo Penc, and Peter Fulde, “Quantum ice: A quantum monte carlo study,” *Phys. Rev. Lett.* **108**, 067204 (2012).
- [17] Yi-Ping Huang, Gang Chen, and Michael Hermele, “Quantum spin ices and topological phases from dipolar-octupolar doublets on the pyrochlore lattice,” *Phys. Rev. Lett.* **112**, 167203 (2014).
- [18] Yasuyuki Kato and Shigeki Onoda, “Numerical evidence of quantum melting of spin ice: Quantum-to-classical crossover,” *Phys. Rev. Lett.* **115**, 077202 (2015).
- [19] Yao-Dong Li, Xiaoqun Wang, and Gang Chen, “Hidden multipolar orders of dipole-octupole doublets on a triangular lattice,” *Phys. Rev. B* **94**, 201114 (2016).
- [20] Yao-Dong Li and Gang Chen, “Symmetry enriched  $U(1)$  topological orders for dipole-octupole doublets on a pyrochlore lattice,” *Phys. Rev. B* **95**, 041106 (2017).
- [21] Lucile Savary and Leon Balents, “Disorder-induced quantum spin liquid in spin ice pyrochlores,” *Phys. Rev. Lett.* **118**, 087203 (2017).
- [22] Z. Hao J. Carrasquilla and R. G. Melko, “A two-dimensional spin liquid in quantum kagome ice,” *Nature communications* **6**, 7421 (2015).
- [23] Wojciech Hubert Zurek, “Decoherence, einselection, and the quantum origins of the classical,” *Rev. Mod. Phys.* **75**, 715–775 (2003).
- [24] S. V. Isakov, S. Wessel, R. G. Melko, K. Sengupta, and Yong Baek Kim, “Hard-core bosons on the kagome lattice: Valence-bond solids and their quantum melting,” *Phys. Rev. Lett.* **97**, 147202 (2006).
- [25] Kedar Damle and T. Senthil, “Spin nematics and magnetization plateau transition in anisotropic kagome magnets,” *Phys. Rev. Lett.* **97**, 067202 (2006).
- [26] Yi-Ping Huang and Michael Hermele, “Theory of quantum kagome ice and vison zero modes,” *Phys. Rev. B* **95**, 075130 (2017).
- [27] Alexei Kitaev and John Preskill, “Topological entanglement entropy,” *Phys. Rev. Lett.* **96**, 110404 (2006).
- [28] Michael Levin and Xiao-Gang Wen, “Detecting topological order in a ground state wave function,” *Phys. Rev. Lett.* **96**, 110405 (2006).
- [29] Eric Rowell, Richard Stong, and Zhenghan Wang, “On classification of modular tensor categories,” *Communications in Mathematical Physics* **292**, 343–389 (2009).
- [30] Hong-Chen Jiang, Zhenghan Wang, and Leon Balents, “Identifying topological order by entanglement entropy,” *Nature Physics* **8**, 902 EP – (2012).
- [31] Matthew B. Hastings and Roger G. Melko Sergei V. Isakov, “Topological entanglement entropy of a bose-hubbard spin liquid,” *Nature* **7**, 772 (2011).
- [32] J. Ignacio Cirac, Didier Poilblanc, Norbert Schuch, and Frank Verstraete, “Entanglement spectrum and boundary theories with projected entangled-pair states,” *Phys. Rev. B* **83**, 245134 (2011).
- [33] Ryuji Higashinaka, Hideto Fukazawa, and Yoshiteru Maeno, “Anisotropic release of the residual zero-point entropy in the spin ice compound  $\text{Dy}_2\text{Ti}_2\text{O}_7$ : Kagome ice behavior,” *Phys. Rev. B* **68**, 014415 (2003).
- [34] Matthias Troyer, Fabien Alet, and Stefan Wessel, “Histogram methods for quantum systems: from reweighting to Wang-Landau sampling,” *Brazilian Journal of Physics* **34**, 377 – 383 (2004).
- [35] J. Villain, R. Bidaux, J.-P. Carton, and R. Conte, “Order as an effect of disorder,” *Journal de Physique* **41**, 1263–1272 (1980).
- [36] Lucile Savary, Kate A. Ross, Bruce D. Gaulin, Jacob P. C. Ruff, and Leon Balents, “Order by quantum disorder in  $\text{Er}_2\text{Ti}_2\text{O}_7$ ,” *Phys. Rev. Lett.* **109**, 167201 (2012).
- [37] M. E. Zhitomirsky, M. V. Gvozdikova, P. C. W. Holdsworth, and R. Moessner, “Quantum order by disorder and accidental soft mode in  $\text{Er}_2\text{Ti}_2\text{O}_7$ ,” *Phys. Rev. Lett.* **109**, 077204 (2012).
- [38] Doron L Bergman, Ryuichi Shindou, Gregory A Fiete, and Leon Balents, “Effective hamiltonians for some highly frus-

- trated magnets,” *Journal of Physics: Condensed Matter* **19**, 145204 (2007).
- [39] Doron L. Bergman, Ryuichi Shindou, Gregory A. Fiete, and Leon Balents, “Degenerate perturbation theory of quantum fluctuations in a pyrochlore antiferromagnet,” *Phys. Rev. B* **75**, 094403 (2007).
- [40] E. Lhotel, S. Petit, M. Ciomaga Hatnean, J. Ollivier, H. Mutka, E. Ressouche, M. R. Lees, and G. Balakrishnan, “Dynamic quantum kagome ice,” (2017), arXiv:1712.02418 [cond-mat].
- [41] Jeffrey G. Rau and Michel J. P. Gingras, “Magnitude of quantum effects in classical spin ices,” *Phys. Rev. B* **92**, 144417 (2015).
- [42] C.-J. Huang, C. Liu, Z. Meng, Y. Yu, Y. Deng, and G. Chen, “Extended Coulomb liquid of paired hardcore boson model on a pyrochlore lattice,” (2018), arXiv:1806.04014 [cond-mat.str-el].
- [43] Anders W. Sandvik and Juhani Kurkijärvi, “Quantum Monte Carlo simulation method for spin systems,” *Phys. Rev. B* **43**, 5950–5961 (1991).
- [44] Olav F. Syljuasen and Anders W. Sandvik, “Quantum Monte Carlo with directed loops,” *Phys. Rev. E* **66**, 046701 (2002).
- [45] Roger G. Melko, Ann B. Kallin, and Matthew B. Hastings, “Finite-size scaling of mutual information in Monte Carlo simulations: Application to the spin- $\frac{1}{2}$  XXZ model,” *Phys. Rev. B* **82**, 100409 (2010).
- [46] Roger G Melko, “Simulations of quantum XXZ models on two-dimensional frustrated lattices,” *Journal of Physics: Condensed Matter* **19**, 145203 (2007).

### Appendix A: Degenerate perturbation theory

We start from the classical part in the XYZh model, denoted as  $H_0$ ,

$$\begin{aligned} H &= H_0 + V \\ H_0 &= J_z \sum_{\langle i,j \rangle} S_z^i S_z^j - h \sum_i S_z^i. \end{aligned} \quad (\text{A1})$$

where the off-diagonal term corresponds to the ring-exchange process that acts on hexagons with  $n = 3$ , and the diagonal terms correspond to processes that  $V$  acts on each bond only once on hexagons with  $n \geq 4$  (see Fig. 6, 7, 8). Prefactors associated with each term can be computed by listing all possible ways to arrange the local two-site ( $S^\pm S^\pm$  or  $S^\pm S^\mp$ ) operators ( $G$ ) to form the perturbation operators  $H_\square$  that transfer states within the ice manifold [38, 39].

We treat the quantum term  $V$  as perturbation acting on the degenerate classical ice manifold  $\Omega$  with the ice rule ”2-up-1-down” ( $h > 0$ ) or ”2-down-1-up” ( $h < 0$ ),

$$H_0 \Omega = E_0 \Omega. \quad (\text{A2})$$

Define an operator  $\mathbb{P}$  that projects the states  $\Psi$  in the Hilbert space to the degenerate ice manifold,

$$\mathbb{P} \Psi = \Omega \quad (\text{A3})$$

The perturbation expansion can be written as,

$$\begin{aligned} (H_0 + \mathbb{P} V \sum_{t=0}^{\infty} G^t \mathbb{P}) \Psi &= E \Omega \\ G &= \frac{(I - \mathbb{P})}{E - H_0} V \end{aligned} \quad (\text{A4})$$

We now have a non-linear eigenvalue problem to solve for the energy shifts ( $\epsilon = E - E_0$ ),

$$\hat{P} \Omega = \epsilon \Omega, \quad (\text{A5})$$

where

$$\hat{P} \equiv \left( V \sum_{t=0}^{\infty} G^t \right). \quad (\text{A6})$$

Essentially, perturbations coming from the quantum fluctuations lift the degeneracy of the ice manifold and quantum phase emerges. In the following calculation, we use hexagon units as defined in the main text and take  $h > 0$ , where all the triangular plaques follows ”2-up-1-down” rule.

For the case that the  $S^\pm S^\pm$  is the only present quantum fluctuation, the lowest non-constant term is at the sixth order,

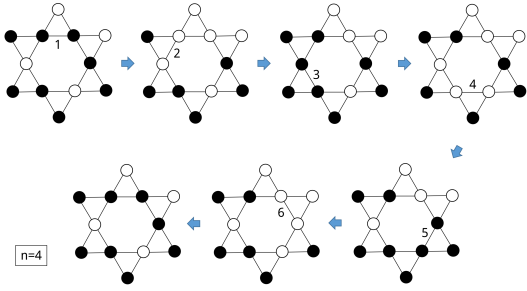
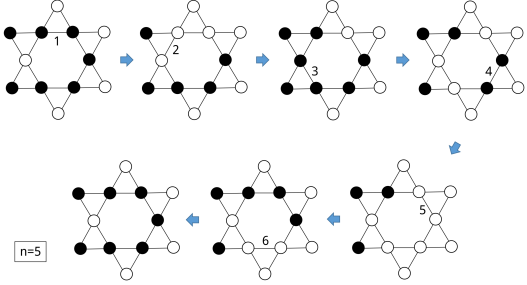
$$V G^5 \equiv \hat{P}_6, \quad (\text{A7})$$

which is the sum of off-diagonal  $H_o$  and diagonal  $H_d$  contributions.

$$\begin{aligned} \hat{P}_6 &= H_d + H_o \\ &= D_4 \sum_{\forall \square n=4} H_\square + D_5 \sum_{\forall \square n=5} H_\square + D_6 \sum_{\forall \square n=6} H_\square + K_{pp} \sum_{\forall \square n=3} H_\square, \end{aligned} \quad (\text{A8})$$

The prefactors for the off-diagonal ring-exchange term,

$$K_{pp} = -\frac{6J_{\pm\pm}^6}{J_z^2(2h + J_z)^5} [7J_z^2 + 14J_z h + 8h^2] \quad (\text{A9})$$

FIG. 6: Relevant diagonal process on hexagon with  $n = 4$ FIG. 7: Relevant diagonal process on hexagon with  $n = 5$ 

and diagonal terms

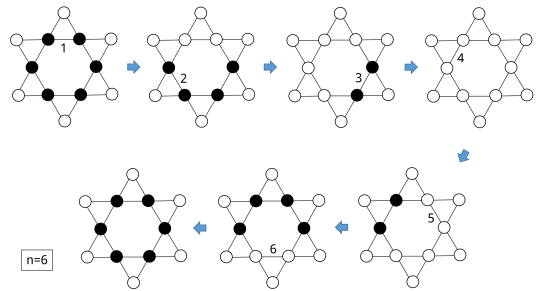
$$\begin{aligned}
 D_4 &= -\frac{J_{\pm\pm}^6}{4hJ_z^2(J_z + 2h)^2} \\
 D_5 &= -J_{\pm\pm}^6 \frac{8J(3J_z + 4h)(2J_z + h) + h(7J_z + 4h)^2}{4hJ_z^2(J_z + 2h)^2(2J_z + h)(3J_z + 4h)^2} \\
 D_6 &= -\frac{12J_{\pm\pm}^6}{(3J_z + 4h)^2(J_z + 2h)(J_z + h)h} \quad (\text{A10})
 \end{aligned}$$

If we further let  $h = J_z$  provided the system is within the lobe, we obtain,

$$\begin{aligned}
 K_{pp} &= -\frac{58}{81} \frac{J_{\pm\pm}^6}{J_z^5} \\
 D_4 &= -\frac{1}{36} \frac{J_{\pm\pm}^6}{J_z^5} \\
 D_5 &= -\frac{289}{5292} \frac{J_{\pm\pm}^6}{J_z^5} \\
 D_6 &= -\frac{2}{49} \frac{J_{\pm\pm}^6}{J_z^5} \quad (\text{A11})
 \end{aligned}$$

### Appendix B: Thermal entropy measurement using Wang-Landau method

In general, one can estimate thermal entropy by numerically integrating the specific heat data from QMC. However, this approach requires a very accurate estimate of the specific heat and suffers from the integration error due to the discretized temperature intervals. Instead, we use the Wang-Landau sam-

FIG. 8: Relevant diagonal process on hexagon with  $n = 6$ 

pling scheme [34] to directly access the thermal entropy in our QMC simulations.

In the SSE formalism, the partition function is written as,

$$\begin{aligned}
 Z &= \text{Tr}[e^{-\beta H}] \\
 &= \sum_n \frac{(\beta)^n}{n!} \sum_{\phi, a, b} \langle \phi | H_{a_0, b_0} \dots H_{a_n, b_n} | \phi \rangle \\
 &= \sum_n \beta^n S_n \\
 &= \sum_n W(n) \quad (\text{B1})
 \end{aligned}$$

where  $H_{a_i, b_i}$  is the local Hamiltonian. In our simulation, we perform triangle plaquette decomposition of the Hamiltonian as discussed in Ref. [46] and sampling using the directed loop algorithm [44]. We can rewrite Eq. (B1) in a generalized representation with a weighting factor  $g(n)$ ,

$$\begin{aligned}
 Z' &= \sum_n \beta^n S_n g(n) \\
 &= \sum_n W'(n). \quad (\text{B2})
 \end{aligned}$$

In the simulation, we first search for  $g(n)$  such that the modified weight  $W'(n)$  are roughly equal, and then sample  $Z'$  with the modified weight  $W'(n)$ .

The partition function for a range of arbitrary temperatures  $\bar{\beta}$  can be calculated by,

$$Z(\bar{\beta}) = \sum_n \left( \frac{\bar{\beta}}{\beta} \right)^n \frac{W'(n)}{g(n)} \quad (\text{B3})$$

In our simulation, we fix  $\beta = 1$  for convenience. To obtain the estimates for physical observables, we first record the estimates for each observables in each  $n$  separately,

$$\begin{aligned}
 \langle O_n \rangle &= \sum_{n'} O \delta_{n, n'} \frac{W'(n')}{Z'} \\
 \langle I_n \rangle &= \frac{W'(n')}{Z'}. \quad (\text{B4})
 \end{aligned}$$

We reweight the estimates with the set  $\{g(n)\}$  with an unde-

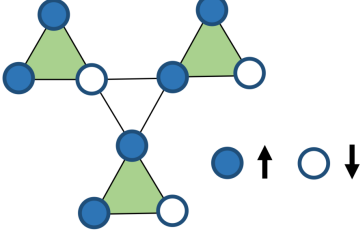


FIG. 9: **Y-star unit for estimate residue entropy.** Each up-triangle satisfies the 2-up-1-down ice rule. In order for the down-triangle to satisfy the ice rule, the number of possible states is reduced from 27 to 12.

terminated constant  $A$ ,

$$\begin{aligned}\langle \bar{O}(\bar{\beta}) \rangle &= A \sum_n \frac{(\bar{\beta})^n}{g(n)} \langle O_n \rangle \\ \langle \bar{Z}(\bar{\beta}) \rangle &= A \sum_n \frac{(\bar{\beta})^n}{g(n)} \langle I_n \rangle\end{aligned}\quad (\text{B5})$$

The observables with arbitrary  $\bar{\beta}$  can be obtained with the relation,

$$\langle O(\bar{\beta}) \rangle = \frac{\langle \bar{O}(\bar{\beta}) \rangle}{\langle \bar{Z}(\bar{\beta}) \rangle}\quad (\text{B6})$$

To determine  $A$ , we use the fact that the  $n = 0$  sector corresponds to a system at infinite temperature ( $\beta \rightarrow 0$ ),

$$A \frac{\langle I_0 \rangle}{g(0)} = 2^N,\quad (\text{B7})$$

where  $N$  is the total number of spins in the system. Using this relation, the physical partition function, free energy and entropy can be calculated,

$$\langle Z(\bar{\beta}) \rangle = \sum_n (\bar{\beta})^n \frac{I_n g(0)}{I_0 g(n)} 2^N\quad (\text{B8})$$

$$\langle F(\bar{\beta}) \rangle = -\frac{1}{\bar{\beta}} \ln [\langle Z(\bar{\beta}) \rangle]\quad (\text{B9})$$

$$\langle S(\bar{\beta}) \rangle = \bar{\beta} [E(\bar{\beta}) - F(\bar{\beta})]\quad (\text{B10})$$

### Appendix C: Residual entropy in classical kagome ice

The residual entropy of the degenerate classical ground states can be estimated by counting the number of spin configurations that satisfy the kagome ice rule. In the following we consider  $h > 0$  and spins should satisfy the 2-up-1-down kagome ice rule on each triangle. Let us focus on the *Y-star* unit with three up-triangles and one down-triangle in the middle. Considering only the up-triangles, the total number of possible states is  $3^{N_p}$ , where  $N_p = N/3$  is the number of up-triangles. However, only twelve out of the 27 possible states are compatible to the "2-up-1-down" rule for the down-triangle. This leads to a reduction factor of  $(\frac{4}{9})^{N_p}$ , and the estimated entropy per spin is  $S/N = 1/3 \ln(4/3)$ .

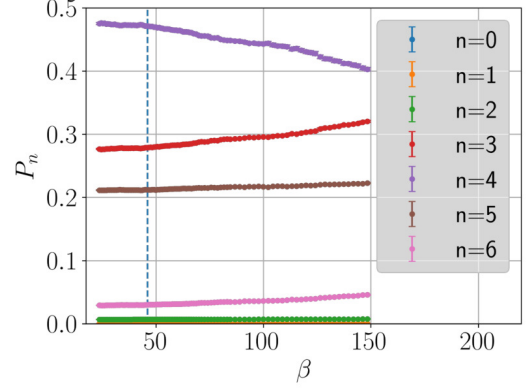


FIG. 10: **Hexagon occupation fraction.** The hexagon fraction in the VBS region with  $h = J_z$ ,  $J_{\pm} = 0.1219J_z$  and  $J_{\pm\pm} = -0.25J_z$ . The vertical blue line indicates the perturbation energy scale.

### Appendix D: Hexagon fraction for $J_{\pm} \neq 0$ and $J_{\pm\pm} \neq 0$

In Fig. 10 we show the QMC results of hexagon fractions  $P_n$  at  $h = J_z$ ,  $J_{\pm} = 0.1219J_z$  and  $J_{\pm\pm} = -0.25J_z$ . The parameters lie in the VBS region with a dominant ring-exchange term as the third-order perturbation. Our result clearly shows the rise of  $P_3$  and the decrease of  $P_4$  at temperature lower than the perturbative energy scale estimated by the ring-exchange process  $\beta \sim \frac{J_z^2}{12J_{\pm}^3} = 46/J_z$ , with the same behaviour as in the XXZ model ( $J_{\pm} \neq 0$ ,  $J_{\pm\pm} = 0$ ).

### Appendix E: Phase diagrams

In Fig. 11 we show the phase diagrams in various planes of the parameter space. To map out the phase boundaries, we take the advantage of the first order transition across the phases. The dramatically change across the first order transition boundaries of the magnetization  $M_z$  and magnetic susceptibility  $\chi_z$ , defined as

$$\begin{aligned}M_z &= \frac{1}{N} \left\langle \sum_i S_i^z \right\rangle, \\ \chi_z &= \left\langle \left( \sum_i S_i^z \right)^2 \right\rangle - \left\langle \sum_i S_i^z \right\rangle^2,\end{aligned}\quad (\text{E1})$$

are used to identify the phase boundaries.

### Appendix F: Structure factors

The three-fold degenerate VBS state with broken translational symmetry can be identified from the peaks of the static structure factor  $S(\mathbf{q})$  at ordering momentum vector  $\mathbf{q} = \langle \frac{2\pi}{3}, 0 \rangle$  and symmetry related momenta. The static structure factor defines as :

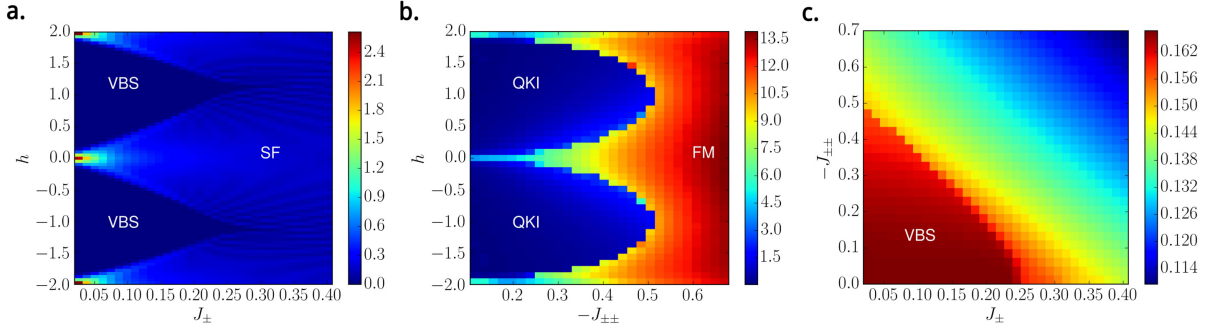


FIG. 11: **Phase diagram in various planes of the parameter space.** **a.** The phase diagram in the  $J_{\pm}$ - $h$  plane. **b.** The phase diagram in the  $J_{\pm\pm}$  -  $h$  plane. **c.** The phase diagram in the  $J_{\pm}$  -  $J_{\pm\pm}$  plane with  $h = 1$ . Simulations are performed with system size  $L = 6$  at temperature  $T = 0.015J_z$  using standard SSE.

$$f(\mathbf{q}) = \frac{1}{N} \sum_j e^{i\mathbf{q}\cdot\mathbf{r}_j} S_j^z$$

$$S(\mathbf{q}) = \langle f(\mathbf{q})f(-\mathbf{q}) \rangle - \langle f(\mathbf{q}) \rangle \langle f(-\mathbf{q}) \rangle \quad (\text{F1})$$

With  $N = 3 \times L \times L$  is the total number of spins. Fig. 12 shows the line cut of the structure factors for different phases along  $\mathbf{q} = (q_x, 0)$  of Fig. 5 in the main text. In both VBS-a and VBS-b cases, peaks at  $\mathbf{q} = \langle \frac{2\pi}{3}, 0 \rangle$  emerge out of the background.

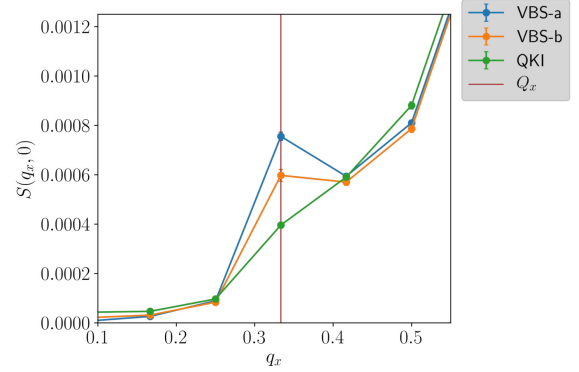


FIG. 12: **Structure factors in various phases.** The structure factors are measured at  $N = 3 \times 12 \times 12$  at  $T = 0.02$ . The  $x$  component momentum vector  $q_x$  are in unit of  $2\pi$ .  $Q_x = \frac{2\pi}{3}$  indicates the VBS ordering vector.